

Observational Constraints on Oscillating Dark-Energy Parametrizations

Supriya Pan^a Emmanuel N. Saridakis^{b,c,d} Weiqiang Yang^e

^a*Department of Mathematics, Raiganj Surendranath Mahavidyalaya, Sudarshanpur, Raiganj, Uttar Dinajpur, West Bengla 733134, India*

^b*Chongqing University of Posts & Telecommunications, Chongqing, 400065, China*

^c*Physics Division, National Technical University of Athens, 15780 Zografou Campus, Athens, Greece*

^d*CASPER, Physics Department, Baylor University, Waco, TX 76798-7310, USA*

^e*Department of Physics, Liaoning Normal University, Dalian, 116029, P. R. China*

E-mail: span@research.jdvu.ac.in, Emmanuel_Saridakis@baylor.edu, d11102004@163.com

ABSTRACT: We perform a detailed confrontation of various oscillating dark-energy parametrizations with the latest sets of observational data. In particular, we use data from Joint Light Curve analysis (JLA) sample from Supernovae Type Ia, Baryon Acoustic Oscillations (BAO) distance measurements, Cosmic Microwave Background (CMB) observations, redshift space distortion, weak gravitational lensing, Hubble parameter measurements from cosmic chronometers, and we impose constraints on four oscillating models. From the analyses we find that the best-fit characters of almost all models are bent towards the phantom region, nevertheless in all of them the quintessential regime is also allowed within 1σ confidence-level. Furthermore, the deviations from Λ CDM cosmology are not significant, however for two of the models they could be visible at large scales, through the impact on the temperature anisotropy of the CMB spectra and on the matter power spectra. Finally, we perform the Bayesian analysis, which shows that the current observational data support the Λ CDM paradigm over this set of oscillating dark-energy parametrizations.

KEYWORDS: Dark Energy, Observational Constraints, Oscillating Parametrizations

Contents

| | | |
|----------|---|-----------|
| 1 | Introduction | 1 |
| 2 | Cosmological equations: Background and perturbations | 2 |
| 3 | Oscillating Dark-Energy models | 4 |
| 4 | Observational Data | 5 |
| 5 | Observational constraints | 8 |
| 5.1 | Model I | 9 |
| 5.2 | Model II | 11 |
| 5.3 | Model III | 14 |
| 5.4 | Model IV | 14 |
| 6 | Statistical Model Comparison: Bayesian Evidence | 16 |
| 7 | Conclusions | 19 |

1 Introduction

The universe acceleration at late times is one of the most interesting findings of modern cosmology, and thus there are two main directions that one could follow to explain it. The first way is to keep general relativity as the gravitational theory and introduce new components, that go beyond the Standard Model of Particle Physics, collectively known as the dark energy sector [1, 2]. The second way is to construct a modified gravitational theory, whose additional degrees of freedom can drive the universe acceleration [3–5].

At the phenomenological level both the above approaches lead to a specific universe accelerated expansion, that can be quantified by the evolution of the (effective in the case of modified gravity) dark energy equation-of-state parameter. Hence, parametrizations of the dark energy fluid can lead to reconstructions of the universe late-time expansion. The basic idea relies on the fact that the dark energy equation-of-state parameter $w_x = p_x/\rho_x$, with ρ_x and p_x the dark energy energy density and pressure respectively, can be parametrized using different functional forms in terms of the cosmological redshift.

In principle, there is not a theoretical guiding rule to select the best $w_x(z)$, however using observational data it is possible to find viable parametrizations. In the literature one can find many parametric dark energy models, that have been introduced and fitted with observational data: (i) one-parameter family of dark energy models [6] (ii) two-parameters family of dark energy parametrizations, namely, Chevallier-Polarski-Linder parametrization [7, 8], Linear parametrization [9–11], Logarithmic parametrization

[12], Jassal-Bagla-Padmanabhan parametrization [13], Barboza-Alcaniz parametrization [14], etc (see [15–25]), (iii) three-parameters family of dark energy parametrizations [26], and (iv) four-parameters family of dark energy parametrizations [26–28].

One of the interesting parametrizations is the class of models in which $w_x(z)$ exhibits oscillating behaviour [25, 29–39]. The oscillating dark energy models are appealing and prove to lead to desirable cosmological behaviour. In particular, they can alleviate the coincidence problem, since they may lead to both accelerating and decelerating phases in a periodic manner [30], and thus to dark matter and dark energy density parameters of the same order. Furthermore, one can construct oscillating dark energy models that can unify the current acceleration with the early-time inflationary phase [31].

The main question that arises naturally is whether oscillating dark-energy models are in agreement with the latest observational data. Although an early, basic fitting was performed in [40], such an investigation has not been fulfilled in detail. In the present work we are interested in performing a complete observational confrontation, in order to examine whether oscillating dark energy models are in agreement with the latest data, namely: Joint Light Curve analysis sample from Supernovae Type Ia, Baryon Acoustic Oscillations (BAO) distance measurements, Cosmic Microwave Background (CMB) observations, redshift space distortion, weak gravitational lensing, Hubble parameter measurements from cosmic chronometers, and finally the local Hubble constant value.

The manuscript is organized in the following way. In Section 2 we present the cosmological equations for a dark energy model, both at background and perturbative levels. In Section 3 we introduce the oscillating dark energy models, through suitable parametrizations of the dark-energy equation-of-state parameter. In Section 4 we present the various observational data sets that we will use in our analysis, and in Section 5 we perform a detailed observational confrontation for various oscillating models. In Section 6 we compare the results for all models, both amongst each other as well as relating to w CDM and Λ CDM cosmology. Finally, Section 7 is devoted to the Conclusions.

2 Cosmological equations: Background and perturbations

In this section we provide the basic equations, both at the background and at the perturbation level, of a general cosmological scenario. Throughout the work we consider the homogeneous and isotropic Friedmann-Lemaître-Robertson-Walker (FLRW) metric of the form

$$ds^2 = -dt^2 + a^2(t) \left[\frac{dr^2}{1 - kr^2} + r^2 (d\theta^2 + \sin^2 \theta d\phi^2) \right], \quad (2.1)$$

where $a(t)$ is the scale factor and $k = -1, +1, 0$ corresponds respectively to open, closed and flat geometry. For simplicity, in the following we focus on the flat geometry, as it is favored by observations, although the analysis can be straightforwardly extended to the non-flat case too. The Friedmann equations are extracted as

$$H^2 + \frac{k}{a^2} = \frac{8\pi G}{3} \rho_{tot}, \quad (2.2)$$

$$2\dot{H} + 3H^2 + \frac{k}{a^2} = -8\pi G p_{tot}, \quad (2.3)$$

where $H = \dot{a}/a$ is the Hubble function and dots denote derivatives with respect to the cosmic time, t . In the above equations ρ_{tot} and p_{tot} are respectively the total energy density and pressure of the universe content, considered to be effectively described by perfect fluids. In particular, we consider that the universe consists of radiation, baryonic matter, dark matter and (effective) dark energy, and therefore the total energy density and the total pressure of the universe read as $\rho_{tot} = \rho_r + \rho_b + \rho_c + \rho_x$ and $p_{tot} = p_r + p_b + p_c + p_x$, where ρ_r, p_r correspond to radiation, ρ_b, p_b to baryonic sector, ρ_c, p_c to dark matter, and ρ_x, p_x to the dark energy sector. If we additionally assume that these sectors do not mutually interact, then each one is separately conserved, namely it satisfies

$$\dot{\rho}_i + 3H(1 + w_i)\rho_i = 0, \quad (2.4)$$

where $w_i \equiv p_i/\rho_i$ is the i -th component's equation-of-state parameter. Since radiation has $w_r = 1/3$, we obtain $\rho_r \propto (a/a_0)^{-4}$. Similarly, since as usual the baryonic and dark matter sectors are considered to be pressureless, we obtain $\rho_b \propto (a/a_0)^{-3}$ and $\rho_c \propto (a/a_0)^{-3}$, with a_0 the current value of the scale factor. Finally, since the dark energy fluid has a general equation-of-state parameter $w_x \equiv p_x/\rho_x$, its evolution equation leads to

$$\rho_x = \rho_{x,0} \left(\frac{a}{a_0}\right)^{-3} \exp\left(-3 \int_{a_0}^a \frac{w_x(a')}{a'} da'\right). \quad (2.5)$$

Hence, we can see that the evolution of the dark energy fluid is obviously highly dependent on the form of $w_x(a)$.

Let us now investigate the perturbations of the above general cosmological scenario. The perturbation equations of a general dark energy scenario have been explored in detail in the literature [1]. We choose the synchronous gauge, and thus the perturbed FLRW metric takes the form

$$ds^2 = a^2(\tau) [-d\tau^2 + (\delta_{ij} + h_{ij})dx^i dx^j], \quad (2.6)$$

where τ is the conformal time, and where δ_{ij}, h_{ij} are respectively the unperturbed and the perturbed metric tensors. Now, for the perturbed FLRW metric (2.6), using the conservation equation for the energy-momentum tensor of the i -th fluid, namely $T_{;\nu}^{\mu\nu} = 0$, one can conveniently write down the Einstein's equations in the two gauges, namely, the conformal Newtonian gauge or in the synchronous gauges of the Fourier space κ . We choose the latter gauge, and in that gauge, one can obtain the continuity and the Euler equations as [41–43]:

$$\delta'_i = -(1 + w_i) \left(\theta_i + \frac{h'}{2}\right) - 3\mathcal{H} \left(\frac{\delta p_i}{\delta \rho_i} - w_i\right) \delta_i - 9\mathcal{H}^2 \left(\frac{\delta p_i}{\delta \rho_i} - c_{a,i}^2\right) (1 + w_i) \frac{\theta_i}{\kappa^2}, \quad (2.7)$$

$$\theta'_i = -\mathcal{H} \left(1 - 3\frac{\delta p_i}{\delta \rho_i}\right) \theta_i + \frac{\delta p_i / \delta \rho_i}{1 + w_i} \kappa^2 \delta_i - \kappa^2 \sigma_i, \quad (2.8)$$

where the prime denotes differentiation with respect to the conformal time τ . In these equations $\delta_i = \delta\rho_i/\rho_i$ is the density perturbation, $\mathcal{H} = a'/a$, is the conformal Hubble factor, $h = h_j^j$ is the trace of the metric perturbations h_{ij} , and $\theta_i \equiv i\kappa^j v_j$ is the divergence of the i -th fluid velocity. Additionally, σ_i is the anisotropic stress of the i -th fluid, which will be neglected in our analysis. Finally, $c_{a,i}^2 = \dot{p}_i/\dot{\rho}_i$ is the adiabatic speed of sound of the i -th fluid. As it is known, for an imperfect fluid the quantity $c_s^2 = \delta p_i/\delta\rho_i$ is the sound speed for the i -th fluid. Thus, the adiabatic sound speed is related to the sound speed through

$$c_{a,i}^2 = w_i - \frac{w_i'}{3\mathcal{H}(1+w_i)}. \quad (2.9)$$

We mention here that many dark energy models can be described through imperfect fluids, which have $c_s^2 = 1$ while c_a could be different [44–46]. Hence, although there exist models with $c_s^2 > 1$ (e.g in k -essence models), in our analysis we fix this quantity to be unity.

3 Oscillating Dark-Energy models

In this section we consider dark energy parametrizations that exhibit oscillating behaviour with the evolution of the universe. Our primary intention is to investigate these models with current cosmological data.

For convenience we will use as independent variable the redshift, defined as $z = \frac{a_0}{a} - 1$, with the current scale factor a_0 set to 1 for simplicity. We will study the following four models:

- Model I: The first model in this class is

$$w_x(z) = w_0 + b \{1 - \cos[\ln(1+z)]\}, \quad (3.1)$$

where w_0 is the current value of $w_x(z)$ and b is the model parameter. The free parameter b quantifies the dynamical character of the model. For $b = 0$ we acquire $w_x(z) = w_0$, while any nonzero value of b corresponds to a deviation of the model from the constant dark-energy equation-of-state parameter. Let us note that the generalized version of (3.1) can be found in [31], which however allows a large number of parameters in terms of the frequency or period of the oscillations. The inclusion of several free parameters – such as the frequency or period of the oscillations – may add different aspects and richer behavior to the oscillating dark energy models, however, from the statistical point of view, the presence of a large number of free parameters in a dark energy model increases the degeneracy amongst them. The two-parameters models, on the other hand, are able to retain the oscillating features of the parametric dark energy models, whose study is the field of interest of the present work, and qualitatively they look similar to the four-parameters models [31]. Thus, although the four-parameters oscillating dark energy models are the general ones, here we restrict to models with only two free parameters in order to examine if an oscillating behavior is allowed in the dark-energy equation of state, and quantitatively confront it with the observational data. This may serve as a good starting point towards the analysis of the most general oscillating dark energy models.

- Model II: In similar lines we introduce another oscillating function as

$$w_x(z) = w_0 + b \sin[\ln(1+z)], \quad (3.2)$$

with w_0 and b the model parameters as described for Model I. A general version of the above model can be found in [33, 34] in which the authors have considered the period of oscillations along with other free parameters, thus leading to an extended parameter space. Since a large number of parameters generally leads to degeneracy amongst them, in this work we consider the two-parameter model.

- Model III: Another oscillatory dark energy parametrization is [25]

$$w_x(z) = w_0 + b \left[\frac{\sin(1+z)}{1+z} - \sin 1 \right], \quad (3.3)$$

with w_0 and b the model parameters with as described for Model I.

- Model IV: Finally, we consider a new model

$$w_x(z) = w_0 + b \left[\frac{z}{1+z} \right] \cos(1+z), \quad (3.4)$$

where w_0, b are the free parameters as described above. One may note that the above model might be connected with the CPL model [7, 8] for very low redshifts.

4 Observational Data

In this section we provide the various data sets that we will incorporate in the observational fittings. We will use data from the following probes:

1. *Supernovae Type Ia*: We include the latest Joint Light Curve analysis sample [47] from Supernovae Type Ia, one of the cosmological data sets to probe the nature of dark energy. The sample contains 740 number of Supernovae Type Ia data, distributed in the redshift interval $z \in [0.01, 1.30]$. The χ^2 function for this sample becomes

$$\chi_{\text{JLA}}^2 = (\hat{\mu} - \hat{\mu}^m)^T C^{-1} (\hat{\mu} - \hat{\mu}^m), \quad (4.1)$$

where $\hat{\mu}$ is the vector of effective absolute magnitudes, C is the covariance matrix of $\hat{\mu}$ quantifying the statistical and systematic errors (see [47] for details), and $\hat{\mu}^m(z) = 5 \log_{10} \left(\frac{D_L(z)}{10 \text{pc}} \right)$ is the distance modulus at redshift z for the model in which $D_L(z)$ is the luminosity distance [48].

2. *Baryon Acoustic Oscillations (BAO) distance measurements*: For the BAO data, we use the ratio of r_s/D_V acting as a “standard ruler” in which the quantity r_s refers to the comoving sound horizon at the baryon drag epoch and D_V refers to the

effective distance determined by D_A . The angular diameter distance and the Hubble parameter H are related through the following equation [49]

$$D_V(z) = \left[(1+z)^2 D_A(z)^2 \frac{z}{H(z)} \right]^{1/3}. \quad (4.2)$$

We include four measurements of r_s/D_V at four different redshifts, namely from the 6dF Galaxy Survey (6dFGS) measurement at $z_{\text{eff}} = 0.106$ [50], from the Main Galaxy Sample of Data Release 7 of Sloan Digital Sky Survey (SDSS-MGS) at $z_{\text{eff}} = 0.15$ [51], and from the CMASS and LOWZ samples from the latest Data Release 12 (DR12) of the Baryon Oscillation Spectroscopic Survey (BOSS) at $z_{\text{eff}} = 0.57$ and at $z_{\text{eff}} = 0.32$ [52]. The likelihood for BAO is given by

$$\chi_{\text{BAO}}^2 = \sum_i \frac{\left[r_{\text{BAO},i}^{\text{obs}} - r_{\text{BAO},i}^{\text{th}} \right]^2}{\sigma_i^2}, \quad (4.3)$$

where $r_{\text{BAO}} = r_s(z_d)/D_V$ and σ_i 's are the uncertainties in the measurements for each data point $i = 1, 2, 3, 4$, respectively correspond to $z_{\text{eff}} = 0.106$ [50], $z_{\text{eff}} = 0.15$ [51], $z_{\text{eff}} = 0.57$ [52] and $z_{\text{eff}} = 0.32$ [52].

3. *Cosmic Microwave Background (CMB) data:* We incorporate the CMB temperature and polarization anisotropies with their cross-correlations from the Planck Probe [53]. Specifically, we use the combinations of high- and low- ℓ TT likelihoods (overall multiple range $2 \leq \ell \leq 2508$) as well as the combinations of the high- and low- ℓ polarization likelihoods [54], which are notationally referred to as Planck TT, TE, EE+lowTEB. In order to analyze the data we use the publicly available Planck likelihood [54], which eventually marginalizes over several nuisance parameters associated with the measurements. For a detailed study and the implementation of the CMB data, we refer the reader to [53, 54].
4. *Redshift space distortion:* We include two redshift space distortion (RSD) data from CMASS and LowZ galaxy samples. The CMASS sample consists of 777202 galaxies with an effective redshift of $z_{\text{eff}} = 0.57$ [55], while the LOWZ sample contains 361762 galaxies with an effective redshift of $z_{\text{eff}} = 0.32$ [55]. The data-vector containing the cosmological parameters of interest, namely $f(z)\sigma_8(z)$, $H(z)r_s(z_d)$ (in 10^3kms^{-1} units) and $D_A(z)/r_s(z_d)$, reads as

$$D_{\text{data}}(z) = \begin{pmatrix} f(z)\sigma_8(z) \\ H(z)r_s(z_d) \\ D_A(z)/r_s(z_d) \end{pmatrix}. \quad (4.4)$$

The data-vectors for the samples LOWZ and CMASS can be formed as (see Table 3 of [55]):

$$D_{\text{data}}(z_{\text{eff}} = 0.32) = \begin{pmatrix} 0.45960 \\ 11.753 \\ 6.7443 \end{pmatrix}, \quad (4.5)$$

from the LOWZ sample at $k_{\text{max}} = 0.18 h\text{Mpc}^{-1}$, and

$$D_{\text{data}}(z_{\text{eff}} = 0.57) = \begin{pmatrix} 0.41750 \\ 13.781 \\ 9.3276 \end{pmatrix}, \quad (4.6)$$

from the CMASS sample at $k_{\text{max}} = 0.22 h\text{Mpc}^{-1}$. The covariance matrices for the above two samples are given in [55]. In particular, the covariance matrix for the LOWZ sample at $k_{\text{max}} = 0.18 h\text{Mpc}^{-1}$ is

$$C^{\text{LOWZ}} = 10^{-3} \begin{pmatrix} 5.0837 & 23.818 & 10.490 \\ & 300.30 & 73.448 \\ & & 47.493 \end{pmatrix}, \quad (4.7)$$

while the covariance matrix for the CMASS sample at $k_{\text{max}} = 0.22 h\text{Mpc}^{-1}$ is

$$C^{\text{CMASS}} = 10^{-3} \begin{pmatrix} 1.3046 & 4.6434 & 3.5329 \\ & 77.713 & 22.773 \\ & & 21.700 \end{pmatrix}. \quad (4.8)$$

Now, the corresponding likelihood of any cosmological model is given by

$$\mathcal{L} \propto e^{-(D_{\text{data}} - D_{\text{model}})^T C^{-1} (D_{\text{data}} - D_{\text{model}})}, \quad (4.9)$$

where D_{model} represents the vector with the model prediction for the same cosmological parameters as D_{data} and C^{-1} is the inverse of the covariance matrix. Lastly, we mention that when these two RSD data are considered, the BOSS DR12 results will not be considered.

5. *Weak lensing data:* We consider the weak gravitational lensing from the Canada-France-Hawaii Telescope Lensing Survey (CFHTLenS) [56, 57]. The CFHTLenS is the largest weak lensing survey at present and spans 154 square degrees in five optical bands. We use the tomographic CFHTLenS blue galaxy sample for the analysis. In particular, we note that the survey [56], which we follow in this work, uses 21 sets of cosmic shear correlation functions associated with six redshift bins. The weak correlations between the observed shapes of distant galaxies are generally induced due to the weak gravitational lensing by large scale structure. The cosmological information can be extracted through the two-point shear correlation function, which is related to convergence power spectrum

$$P_K^{ij}(l) = \int_0^{\eta_H} d\eta \frac{q_i(\eta)q_j(\eta)}{[f_K(\eta)]^2} P_\delta \left(\frac{l}{f_K(\eta)}; \eta \right), \quad (4.10)$$

where η is the comoving distance, η_H is the horizon distance, and $f_K(\eta)$ is the angular diameter distance out to η . The quantity $f_K(\eta)$ depends on the curvature scalar (k) of spacetime, and q_j is the lensing efficiency function for the redshift bin j (see [56, 57] for more details). The tomographic correlation functions measured from the blue

galaxy sample is consistent with zero intrinsic alignment nuisance parameter A . We use the likelihood analysis of the CFHTLenS data, where the true inverse covariance matrix is given by $\mathbf{C}^{-1} = \alpha_A \hat{\mathbf{C}}^{-1}$. Here $\alpha_A = (n_\mu - p - 2)/(n_\mu - 1)$ and $\hat{\mathbf{C}}$ is the measured covariance matrix in which p is the total number of data points, that is calculated in [56] as follows: for N_t tomographic redshift bins and N_θ angular scales, and considering the shear correlation functions ξ_+^{ij} and ξ_-^{ij} (see [56, 57] for more details) between the redshift bins i, j , we have $p = N_\theta N_t (N_t + 1)$. The quantity n_μ refers to the total number of simulations. The χ^2 function for this data set is given by

$$\chi_{WL}^2 = [\hat{d} - d(\pi)]^T C^{-1} [\hat{d} - d(\pi)], \quad (4.11)$$

where \hat{d} is the vector of measured data points, and $d(\pi)$ represents the vector carrying the model parameters.

6. *Cosmic Chronometers (CC) data:* In our analysis we consider the Hubble parameter values at different redshifts, using the massive and passively evolving galaxies in our universe, known as cosmic chronometers. The measurements of the Hubble parameter values follow the spectroscopic method with high accuracy, and moreover the technique of measurements is model independent [58, 59]. The CC (or $H(z)$) data are compiled in [60], and they contain 30 measurements distributed in the interval $0 < z < 2$. The χ^2 -statistics for the cosmic chronometers data is given by

$$\chi_{CC}^2 = \sum_{i=1}^{30} \frac{(H(z_i) - H_{th}(z_i))^2}{\sigma_i^2}, \quad (4.12)$$

where each z_i with its corresponding uncertainty σ_i can be found in Table 4 of [60].

5 Observational constraints

In this section we proceed to the detailed confrontation of the above oscillating dark energy models with observational data. We perform a combined analysis JLA + BAO + Planck TT, TE, EE + LowTEB (CMB) + RSD + WL+ CC to constrain the proposed oscillating dark energy models (3.1), (3.2), (3.3) and (3.4). Our analysis follows the likelihood $\mathcal{L} \propto \exp(-\chi^2/2)$, where

$$\chi^2 = \chi_{JLA}^2 + \chi_{BAO}^2 + \chi_{CMB}^2 + \chi_{RSD}^2 + \chi_{WL}^2 + \chi_{CC}^2. \quad (5.1)$$

The main statistical analysis is based on the ‘‘Code for Anisotropies in the Microwave Background’’ (CAMB) [61], a publicly available code. For each of the studied models we modify the code accordingly, and then we additionally use CosmoMC, a Markov Chain Monte Carlo (MCMC) simulation, in order to extract the cosmological constraints for the oscillating dark energy models.

In summary, we analyze the following eight-dimensional parameters space:

$$\mathcal{P}_1 \equiv \left\{ \Omega_b h^2, \Omega_c h^2, 100\theta_{MC}, \tau, w_0, b, n_s, \log[10^{10} A_s] \right\}, \quad (5.2)$$

where $\Omega_b h^2$, $\Omega_c h^2$ are respectively the baryon and the cold dark matter density parameter, $100\theta_{MC}$ and τ refer respectively to the ratio of the sound horizon to the angular diameter distance and to the optical depth, n_s and A_s are respectively the scalar spectral index and the amplitude of the initial power spectrum [53], and w_0 and b are the free parameters of the oscillating dark energy models. Additionally, the priors on the cosmological parameters used in the analysis are displayed in Table 1. Lastly, in the following the subscript “0” denotes the value of a quantity at present.

| Parameter | Prior |
|---------------------|--------------|
| $\Omega_c h^2$ | [0.01, 0.99] |
| $\Omega_b h^2$ | [0.005, 0.1] |
| $100\theta_{MC}$ | [0.5, 10] |
| τ | [0.01, 0.8] |
| n_s | [0.5, 1.5] |
| $\log[10^{10} A_s]$ | [2.4, 4] |
| w_0 | [-2, 0] |
| b | [-3, 3] |

Table 1. The flat priors on the cosmological parameters for the CosmoMC analysis.

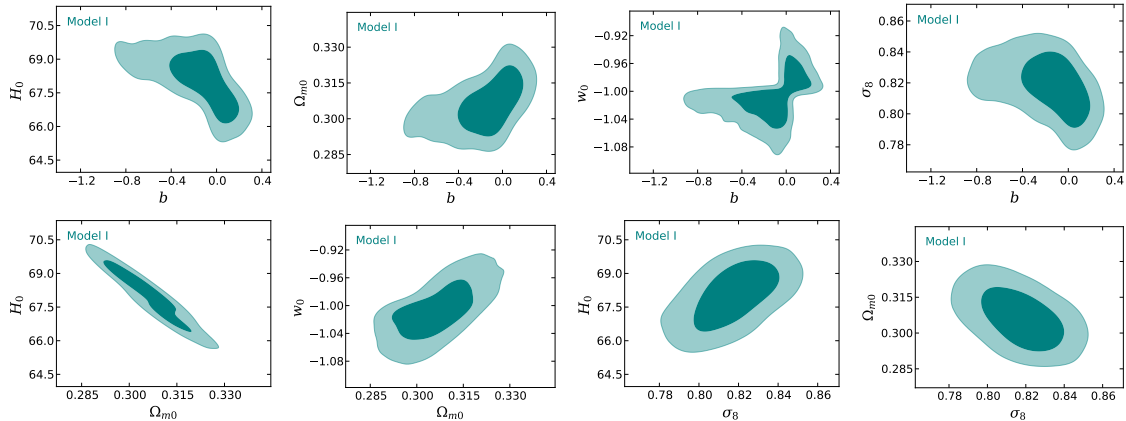


Figure 1. 1σ (68.3%) and 2σ (95.4%) confidence level contour plots for different combinations of the model parameters of Model I (3.1), for the combined observational data JLA + BAO + Planck TT, TE, EE + LowTEB + RSD + WL+ CC. We have defined, $\Omega_{m,0} = \Omega_{c,0} + \Omega_{b,0}$.

In the next subsections we describe the obtained results on each model from this combined analysis.

5.1 Model I

We perform the above combined analysis for the Model I of (3.1), and in Table 2 we summarize the main observational constraints. Furthermore, in Fig. 1 we present the 1σ and 2σ confidence-level contour plots for several combinations of the model parameters and

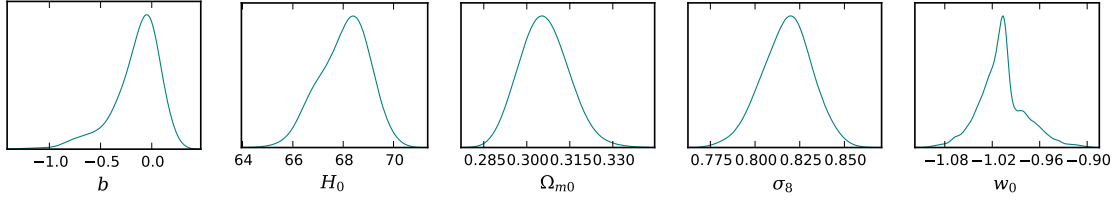


Figure 2. The marginalized 1-dimensional posterior distributions for the model parameters of Model I of (3.1), for the combined observational data JLA + BAO + Planck TT, TE, EE + LowTEB + RSD + WL+ CC.

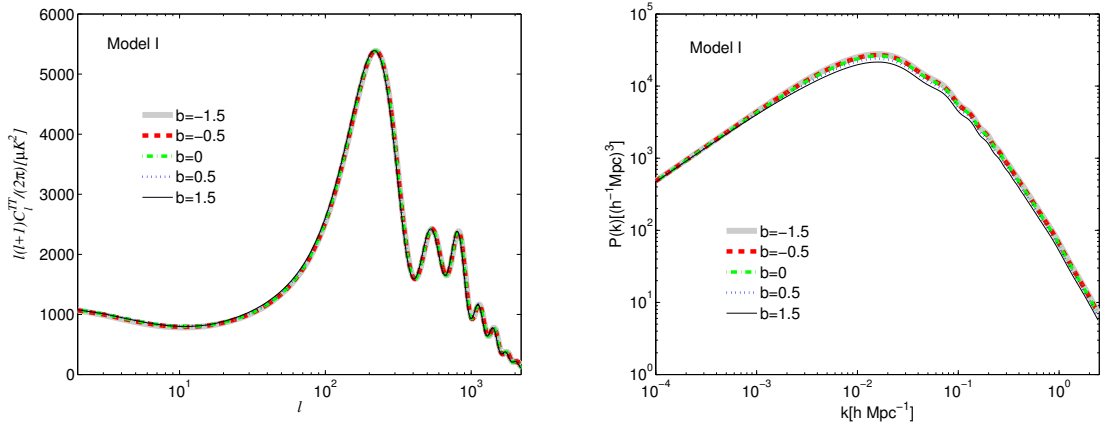


Figure 3. The temperature anisotropy in the CMB spectra (left panel) and the matter power spectra (right panel), for Model I of (3.1), for different values of the parameter b .

| Parameters | Mean $\pm 1\sigma \pm 2\sigma \pm 3\sigma$ | Best fit |
|--------------------|---|----------|
| $\Omega_c h^2$ | $0.1188^{+0.0015+0.0025+0.0031}_{-0.0013-0.0027-0.0035}$ | 0.1187 |
| $\Omega_b h^2$ | $0.02225^{+0.00015+0.00031+0.00038}_{-0.00015-0.00029-0.00038}$ | 0.02218 |
| $100\theta_{MC}$ | $1.04055^{+0.00033+0.00064+0.00086}_{-0.00033-0.00065-0.00085}$ | 1.04054 |
| τ | $0.065^{+0.019+0.038+0.050}_{-0.020-0.038-0.048}$ | 0.065 |
| n_s | $0.9749^{+0.0045+0.0088+0.0120}_{-0.0044-0.0085-0.0107}$ | 0.9726 |
| $\ln(10^{10} A_s)$ | $3.069^{+0.036+0.072+0.094}_{-0.036-0.070-0.091}$ | 3.071 |
| w_0 | $-1.0078^{+0.023+0.068+0.094}_{-0.032-0.059-0.080}$ | -1.0031 |
| b | $-0.1468^{+0.275+0.431+0.511}_{-0.142-0.555-0.803}$ | -0.1127 |
| Ω_{m0} | $0.306^{+0.008+0.017+0.025}_{-0.009-0.017-0.020}$ | 0.308 |
| σ_8 | $0.818^{+0.015+0.027+0.033}_{-0.014-0.029-0.040}$ | 0.817 |
| H_0 | $68.05^{+1.20+1.77+2.25}_{-0.90-2.02-2.68}$ | 67.84 |

Table 2. Summary of the observational constraints on Model I of (3.1), using the observational data JLA + BAO + Planck TT, TE, EE + LowTEB + RSD + WL+ CC. We define $\Omega_{m0} = \Omega_{c0} + \Omega_{b0}$ and we use H_0 to denote the current value of the Hubble function.

of the derived parameters. Similarly, in Fig. 2 we display the marginalized one-dimensional posterior distributions for the involved quantities.

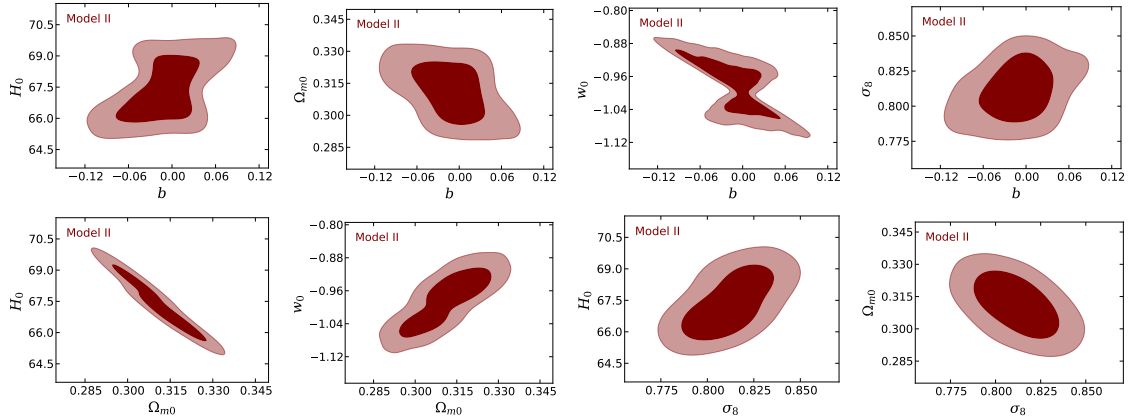


Figure 4. 1σ (68.3%) and 2σ (95.4%) confidence level contour plots for different combinations of the model parameters of Model II of (3.2), for the combined observational data JLA + BAO + Planck TT, TE, EE + LowTEB + RSD + WL+ CC.

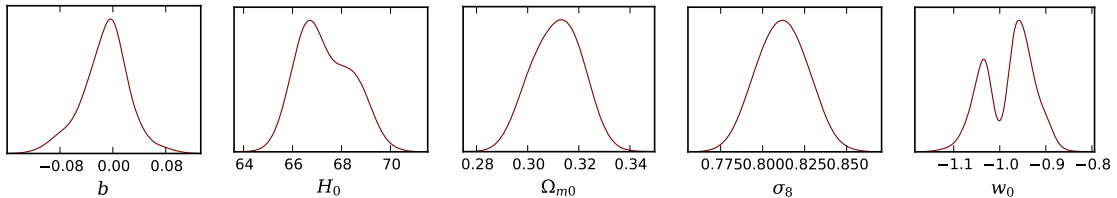


Figure 5. The marginalized 1-dimensional posterior distributions for the model parameters of Model II of (3.2), for the combined observational data JLA + BAO + Planck TT, TE, EE + LowTEB + RSD + WL+ CC.

Our analysis reveals that both the best-fit and the mean values of the dark energy equation-of-state parameter at present (w_0) exhibit phantom behaviour although very close to the cosmological constant boundary, however, as one can see from Table 2, within 1σ confidence-region the quintessential character of w_0 is not excluded.

Additionally, we analyze the behaviour of Model I at large scales through its impact on the temperature anisotropy of the CMB spectra and on the matter power spectra, shown respectively in the upper and lower panel of the Fig. 3, and moreover we compare the results with w CDM cosmology (obtained for $b = 0$). We find that for several values of b we do not find a remarkable behaviour in the CMB spectra. On the other hand, from the matter power spectra we can see that for large positive b values the model has a deviating nature from w CDM cosmology.

In summary, from the observational constraints we deduce that the model is close to w CDM cosmology, and hence to the Λ CDM paradigm too.

5.2 Model II

We perform the combined analysis for the Model II of (3.2), and in Table 3 we summarize the main observational constraints. Additionally, in Fig. 4 we depict the 1σ and 2σ confidence-level contour plots for several combinations of the model parameters and

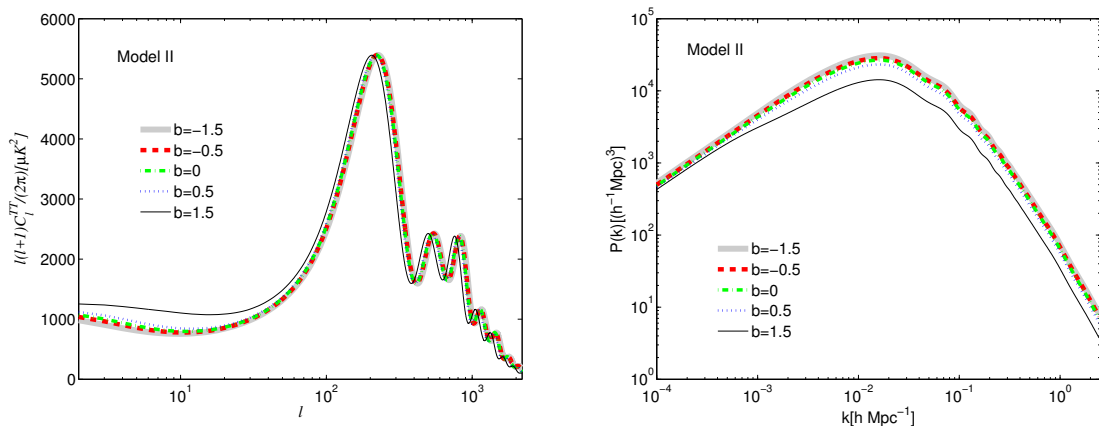


Figure 6. The temperature anisotropy in the CMB spectra (left panel) and the matter power spectra (right panel), for Model II of (3.2), for different values of the parameter b .

the derived parameters, while in Fig. 5 we display the corresponding marginalized one-dimensional posterior distributions for the involved quantities.

| Parameters | Mean $\pm 1\sigma \pm 2\sigma \pm 3\sigma$ | Best fit |
|--------------------|---|----------|
| $\Omega_c h^2$ | $0.1180^{+0.0013+0.0025+0.0033}_{-0.0014-0.0024-0.0031}$ | 0.1190 |
| $\Omega_b h^2$ | $0.02230^{+0.00014+0.00030+0.00048}_{-0.00016-0.00029-0.00039}$ | 0.02218 |
| $100\theta_{MC}$ | $1.04064^{+0.00032+0.00060+0.00079}_{-0.00033-0.00062-0.00081}$ | 1.04048 |
| τ | $0.073^{+0.0185+0.0344+0.0450}_{-0.0187-0.0358-0.0438}$ | 0.060 |
| n_s | $0.9768^{+0.0043+0.0085+0.0111}_{-0.0043-0.0085-0.0107}$ | 0.9736 |
| $\ln(10^{10} A_s)$ | $3.084^{+0.035+0.066+0.087}_{-0.035-0.068-0.085}$ | 3.062 |
| w_0 | $-0.9817^{+0.0535+0.0938+0.1175}_{-0.0616-0.1032-0.1390}$ | -1.0444 |
| b | $-0.0114^{+0.0378+0.0739+0.1001}_{-0.0319-0.0809-0.1071}$ | -0.0144 |
| Ω_{m0} | $0.311^{+0.011+0.019+0.023}_{-0.010-0.019-0.024}$ | 0.300 |
| σ_8 | $0.812^{+0.016+0.029+0.039}_{-0.016-0.029-0.039}$ | 0.823 |
| H_0 | $67.32^{+1.09+2.22+2.86}_{-1.39-1.95-2.37}$ | 68.74 |

Table 3. Summary of the observational constraints on Model II of (3.2) using the observational data JLA + BAO + Planck TT, TE, EE + LowTEB + RSD + WL+ CC.

The joint analysis on Model II shows that the best-fit value of the dark energy equation-of-state parameter w_0 lies in the phantom regime, while the mean value of w_0 exhibits quintessential character. We note that within 1σ confidence-region w_0 can exhibit phantom behaviour, too. However, as we can see from Table 3, w_0 is close to the cosmological constant boundary. Additionally, from the temperature anisotropy in the CMB spectra and the matter power spectra depicted in Fig. 6, we can observe that at large scales this model exhibits a clear deviation from w CDM cosmology (and thus Λ CDM cosmology too) for large positive values of the parameter b .

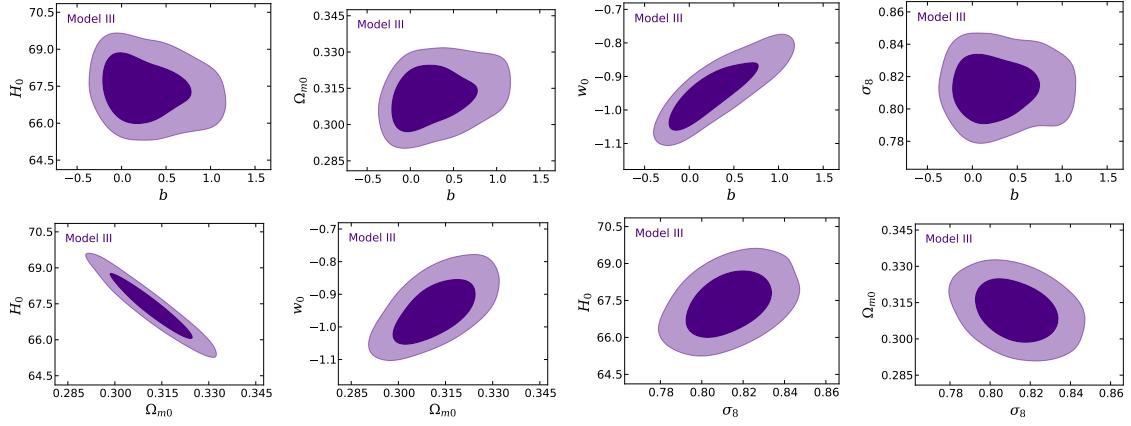


Figure 7. 1σ (68.3%) and 2σ (95.4%) confidence level contour plots for different combinations of the model parameters of Model III of (3.3), for the combined observational data JLA + BAO + Planck TT, TE, EE + LowTEB + RSD + WL+ CC.

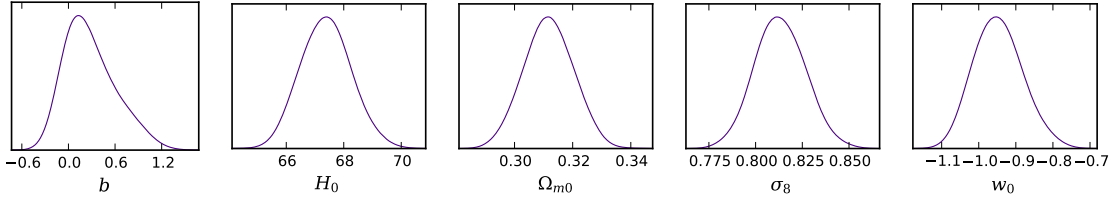


Figure 8. The marginalized 1-dimensional posterior distributions for the model parameters of Model III of (3.3), for the combined observational data JLA + BAO + Planck TT, TE, EE + LowTEB + RSD + WL+ CC.

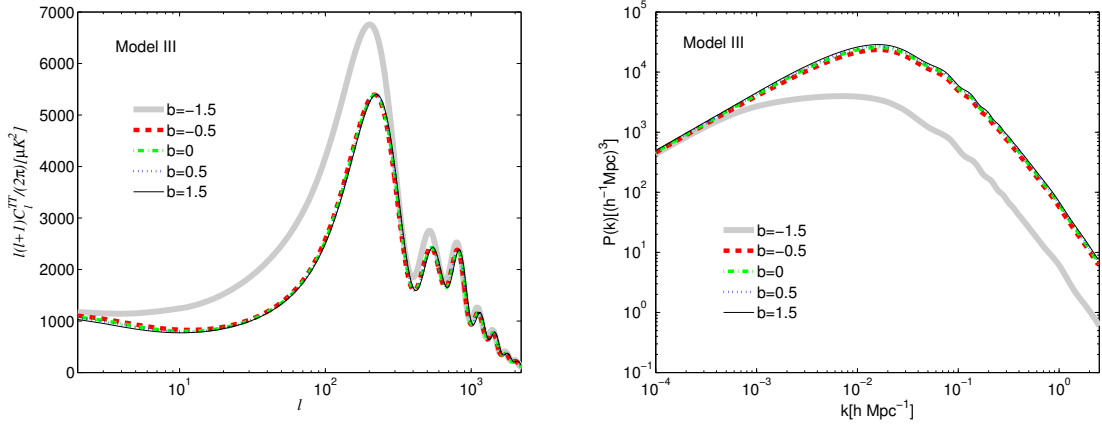


Figure 9. The temperature anisotropy in the CMB spectra (left panel) and the matter power spectra (right panel), for Model III of (3.3), for different values of the parameter b .

| Parameters | Mean $\pm 1\sigma \pm 2\sigma \pm 3\sigma$ | Best fit |
|--------------------|---|----------|
| $\Omega_c h^2$ | $0.1185^{+0.0013+0.0025+0.0033}_{-0.0013-0.0025-0.0033}$ | 0.1182 |
| $\Omega_b h^2$ | $0.02228^{+0.00014+0.00030+0.00038}_{-0.00015-0.00028-0.00036}$ | 0.02229 |
| $100\theta_{MC}$ | $1.04060^{+0.00031+0.00062+0.00079}_{-0.00032-0.00062-0.00077}$ | 1.04065 |
| τ | $0.067^{+0.017+0.034+0.045}_{-0.017-0.035-0.047}$ | 0.083 |
| n_s | $0.9754^{+0.0042+0.0080+0.0108}_{-0.0042-0.0083-0.0105}$ | 0.9777 |
| $\ln(10^{10} A_s)$ | $3.075^{+0.033+0.066+0.088}_{-0.032-0.069-0.093}$ | 3.102 |
| w_0 | $-0.9480^{+0.0631+0.1389+0.1761}_{-0.0749-0.1300-0.1523}$ | -0.8720 |
| b | $0.2700^{+0.2205+0.7261+0.9531}_{-0.4373-0.5691-0.6634}$ | 0.5788 |
| Ω_{m0} | $0.312^{+0.009+0.017+0.021}_{-0.009-0.017-0.021}$ | 0.316 |
| σ_8 | $0.813^{+0.014+0.027+0.037}_{-0.015-0.027-0.035}$ | 0.820 |
| H_0 | $67.38^{+0.88+1.80+2.31}_{-0.91-1.77-2.11}$ | 66.85 |

Table 4. Summary of the observational constraints on Model III of (3.3) using the observational data JLA + BAO + Planck TT, TE, EE + LowTEB + RSD + WL+ CC.

5.3 Model III

We perform the combined analysis described above, for the Model III of (3.3), and in Table 4 we give the summary of the main observational constraints. Furthermore, in Fig. 7 we present the 1σ and 2σ confidence-level contour plots for several combinations of the model parameters and of the derived parameters. Additionally, in Fig. 8 we display the corresponding marginalized one-dimensional posterior distributions for the involved quantities.

According to the joint analysis we find that for Model III, both the best fit and the mean values of the dark-energy equation-of-state parameter at present exhibit quintessential behaviour. However, the 1σ lower confidence level may allow for phantom behavior too, although only slightly. Moreover, from the temperature anisotropy in the CMB spectra and the matter power spectra depicted in Fig. 9, we can see that at large scales, and for large negative values of b (different from Model I and II), the changes in both CMB spectra and matter power spectra, are huge. This implies that this model might exhibit a non-zero deviation from w CDM cosmology and hence from Λ CDM cosmology too. However, from Table 4 we can see that $-0.0721 < b$ at 3σ confidence level, and thus this exotic behaviour is practically not observable. Hence, Model III is practically close to w CDM cosmology, and thus to Λ CDM cosmology too.

5.4 Model IV

Finally, for the Model IV of (3.4) we perform the joint analysis and in Table 5 we display the summary of the main observational constraints. Moreover, in Fig. 10 we show the 1σ and 2σ confidence-level contour plots for several combinations of the model parameters and the derived parameters. Additionally, in Fig. 11 we present the corresponding marginalized one-dimensional posterior distributions for the involved quantities.

| Parameters | Mean $\pm 1\sigma \pm 2\sigma \pm 3\sigma$ | Best fit |
|--------------------|---|----------|
| $\Omega_c h^2$ | $0.1179^{+0.0011+0.0022+0.0031}_{-0.0012-0.0023-0.0029}$ | 0.1182 |
| $\Omega_b h^2$ | $0.02233^{+0.00013+0.00029+0.00040}_{-0.00014-0.00030-0.00035}$ | 0.02216 |
| $100\theta_{MC}$ | $1.04065^{+0.00030+0.00062+0.00081}_{-0.00035-0.00056-0.00074}$ | 1.04056 |
| τ | $0.074^{+0.017+0.032+0.042}_{-0.017-0.032-0.043}$ | 0.056 |
| n_s | $0.9770^{+0.0040+0.0081+0.0111}_{-0.0041-0.0081-0.0110}$ | 0.9763 |
| $\ln(10^{10} A_s)$ | $3.087^{+0.033+0.064+0.082}_{-0.032-0.060-0.084}$ | 3.046 |
| w_0 | $-0.9807^{+0.0333+0.0570+0.0761}_{-0.0360-0.0569-0.0756}$ | -1.0382 |
| b | $0.0544^{+0.0876+0.2324+0.2798}_{-0.0887-0.2142-0.3038}$ | 0.0461 |
| Ω_{m0} | $0.312^{+0.009+0.016+0.020}_{-0.008-0.017-0.020}$ | 0.299 |
| σ_8 | $0.811^{+0.014+0.029+0.038}_{-0.015-0.028-0.038}$ | 0.812 |
| H_0 | $67.26^{+0.83+1.65+2.05}_{-1.02-1.53-1.97}$ | 68.73 |

Table 5. Summary of the observational constraints on Model IV of (3.4) using the observational data JLA + BAO + Planck TT, TE, EE + LowTEB + RSD + WL+ CC.

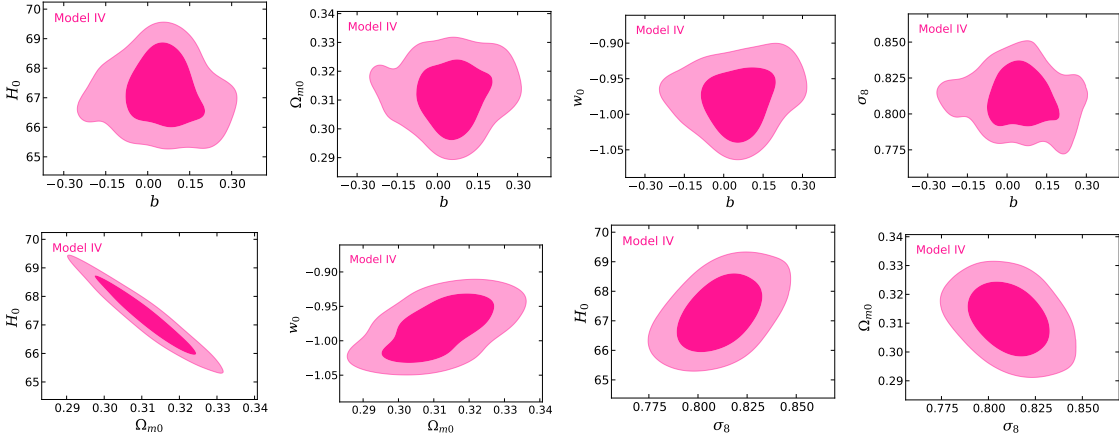


Figure 10. 1σ (68.3%) and 2σ (95.4%) confidence level contour plots for different combinations of the model parameters of Model IV of (3.4), for the combined observational data JLA + BAO + Planck TT, TE, EE + LowTEB + RSD + WL+ CC.

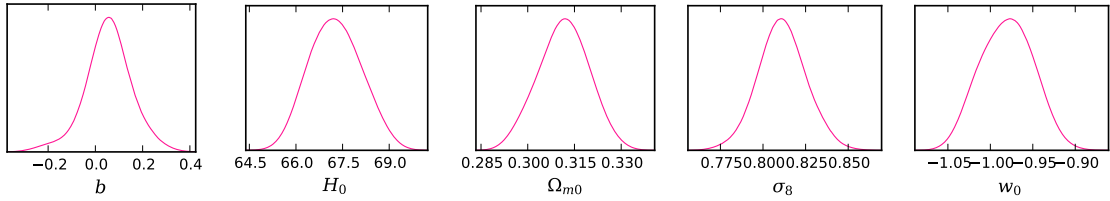


Figure 11. The marginalized 1-dimensional posterior distributions for the model parameters of Model IV of (3.4), for the combined observational data JLA + BAO + Planck TT, TE, EE + LowTEB + RSD + WL+ CC.

As we can observe, the joint analysis reveals that for Model IV, the best-fit value of the dark-energy equation-of-state parameter at present exhibits phantom behaviour, although

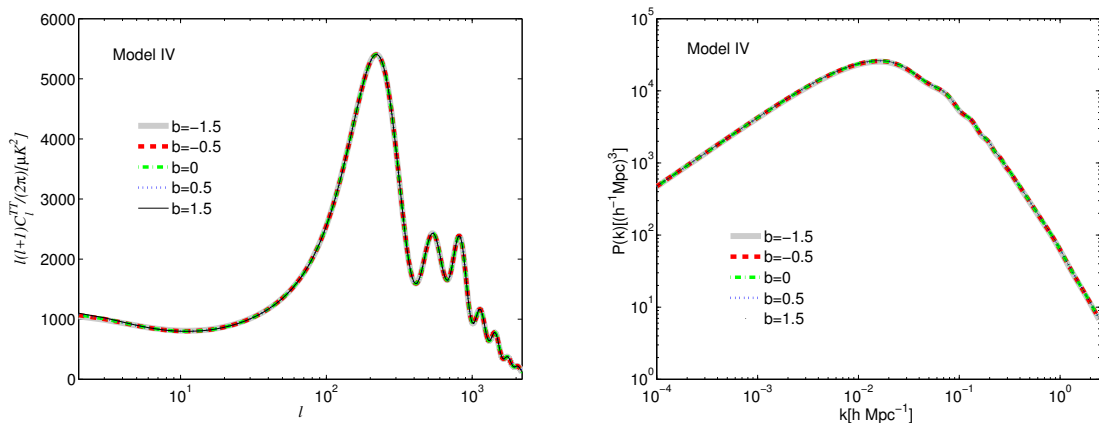


Figure 12. *The temperature anisotropy in the CMB spectra (left panel) and the matter power spectra (right panel), for Model IV of (3.4), for different values of the parameter b .*

very close to -1 , while the mean value of w_0 lies in the quintessence regime. However, as one can see from Table 5, within 1σ confidence-region the phantom character of w_0 is not excluded. Additionally, from the temperature anisotropy in the CMB spectra and the matter power spectra depicted in Fig. 12, we can see that we do not find any significant variation from w CDM cosmology, and thus from Λ CDM paradigm.

We close this section displaying the evolution of the dark-energy equation-of-state parameter of all Models in Fig. 13. This figure shows the qualitative differences between the oscillating dark energy models, both at low- and high- redshifts. From the evolutions of all oscillating dark energy models we find that Model I gives a phantom dark energy during the entire evolution of the universe, while Model II always exhibits a quintessential character. Interestingly, Model III presents a different behaviour: at high redshifts it exhibits a phantom behaviour, while very recently the dark energy equation of state transits from the phantom regime to quintessence one. Concerning Model IV, we find that it exhibits both quintessence and phantom behaviour. In fact, unlike other oscillating dark energy models, it periodically enters into quintessence and phantom region.

6 Statistical Model Comparison: Bayesian Evidence

In this section we perform a statistical comparison of the oscillating dark energy models through the Bayesian evidence, also known as marginal likelihood or model likelihood. The Bayesian evidence plays an important role to compare different cosmological models based on their performance with observational data.

In the Bayesian analysis we need to determine the posterior probability of the model parameters (denoted by θ), given a data set x , any prior information, and a model M . In particular, using Bayes theorem, one can write

$$p(\theta|x, M) = \frac{p(x|\theta, M) \pi(\theta|M)}{p(x|M)}, \quad (6.1)$$

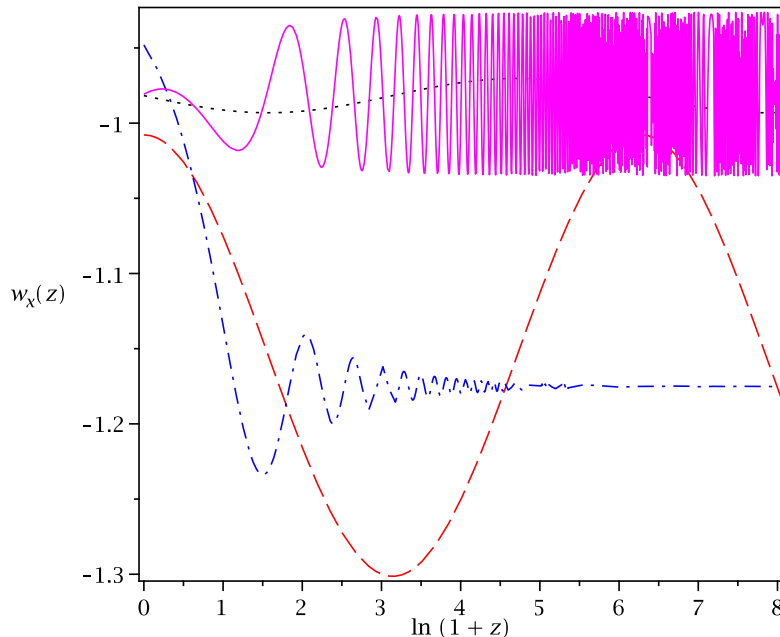


Figure 13. The evolution of the dark-energy equation-of-state parameter $w_x(z)$, has been shown using the mean values of (w_0, b) that arise from the combined analysis *JLA + BAO + Planck TT, TE, EE + LowTEB + RSD + WL+ CC* for Model I of (3.1) (red-dashed), for Model II of (3.2) (black-dotted), for Model III of (3.3) (blue-dash-dotted), and for Model IV of (3.4) (magenta-solid).

where $p(x|\theta, M)$ is the likelihood which is considered to be function of the model parameters θ with the data set fixed, and $\pi(\theta|M)$ is the prior. The denominator $p(x|M)$ in (6.1) is the Bayesian evidence used for the model comparison, and it is the integral over the unnormalised posterior $\tilde{p}(\theta|x, M) \equiv p(x|\theta, M) \pi(\theta|M)$:

$$E \equiv p(x|M) = \int d\theta p(x|\theta, M) \pi(\theta|M), \quad (6.2)$$

and thus it is also referred to as the marginal likelihood. Considering any particular model M_i and the reference model M_j , the posterior probability is thus given by the product of the ratio of the model priors with the ratio of evidences, namely

$$\frac{p(M_i|x)}{p(M_j|x)} = \frac{\pi(M_i)}{\pi(M_j)} \frac{p(x|M_i)}{p(x|M_j)} = \frac{\pi(M_i)}{\pi(M_j)} B_{ij}, \quad (6.3)$$

where $B_{ij} = \frac{p(x|M_i)}{p(x|M_j)}$ is called the Bayes factor of the model M_i relative to the reference model M_j .

For $B_{ij} > 1$ we deduce that the cosmological data employed in the analysis support model M_i more strongly than model M_j . The behaviour of the models can be quantified using different values of B_{ij} (or equivalently $\ln B_{ij}$). In this work, we shall use the widely accepted Jeffreys scales [62], summarized in Table 6, that quantify the viabilities of the models under consideration.

| $\ln B_{ij}$ | Strength of evidence for model M_i |
|-------------------------|--------------------------------------|
| $0 \leq \ln B_{ij} < 1$ | Weak |
| $1 \leq \ln B_{ij} < 3$ | Definite/Positive |
| $3 \leq \ln B_{ij} < 5$ | Strong |
| $\ln B_{ij} \geq 5$ | Very strong |

Table 6. Summary of the revised Jeffreys scale, to quantify the observational support of model M_i with respect to model M_j .

| Model | $\ln B_{ij}$ | Strength of evidence for model Λ CDM |
|-----------|--------------|--|
| Model I | -9.4 | Very Strong |
| Model II | -4.6 | Strong |
| Model III | -6.2 | Very Strong |
| Model IV | -8.4 | Very Strong |

Table 7. Summary of the values of $\ln B_{ij}$, calculated for the oscillating dark energy models with respect to the reference Λ CDM paradigm. According to the Bayesian point of view, the negative values of $\ln B_{ij}$ indicate that Λ CDM is favored over the oscillating dark energy models.

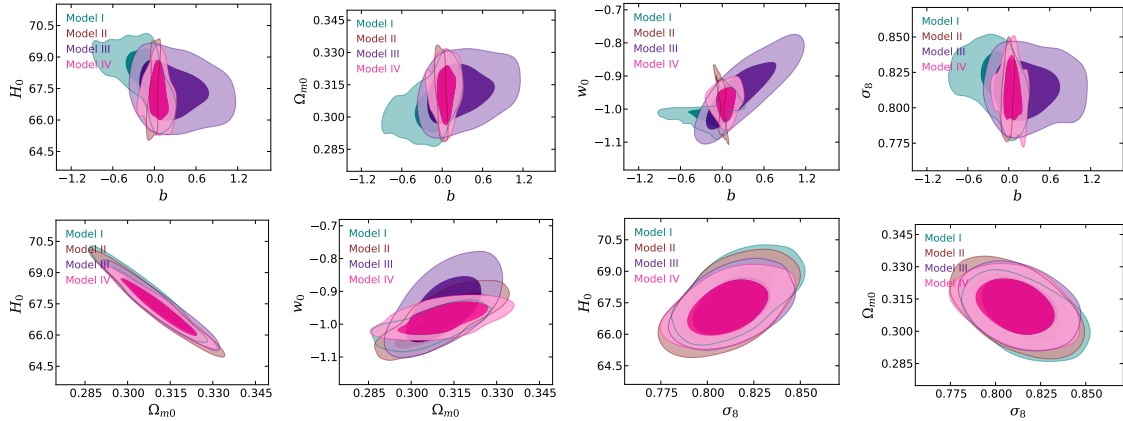


Figure 14. 1σ (68.3%) and 2σ (95.4%) confidence level contour plots for different combinations of the model parameters, for all Models I-IV of (3.1)-(3.4) simultaneously, for the combined observational data JLA + BAO + Planck TT, TE, EE + LowTEB + RSD + WL+ CC.

The Bayesian evidence for the scenarios at hand can be easily calculated, since only the MCMC chains, which are used for parameters estimation, are needed. A detailed explanation can be found in two recent articles [63, 64], where the algorithm that calculates the Bayesian evidence is known as the `MCEvidence` code¹.

Using the `MCEvidence` code we calculate the logarithm of the Bayes factor, i.e. $\ln B_{ij}$, where $i = \text{Model I} - \text{Model IV}$ and $j = \Lambda$ CDM. In Table 7 we summarize the calculated values of $\ln B_{ij}$ for all oscillating dark energy models with respect to the base Λ CDM. For Models I, III and IV we find that $|\ln B_{ij}| > 5$. In particular, we see that $\ln B_{ij} = -9.4$

¹This code is publicly available at github.com/yabebalFantaye/MCEvidence.

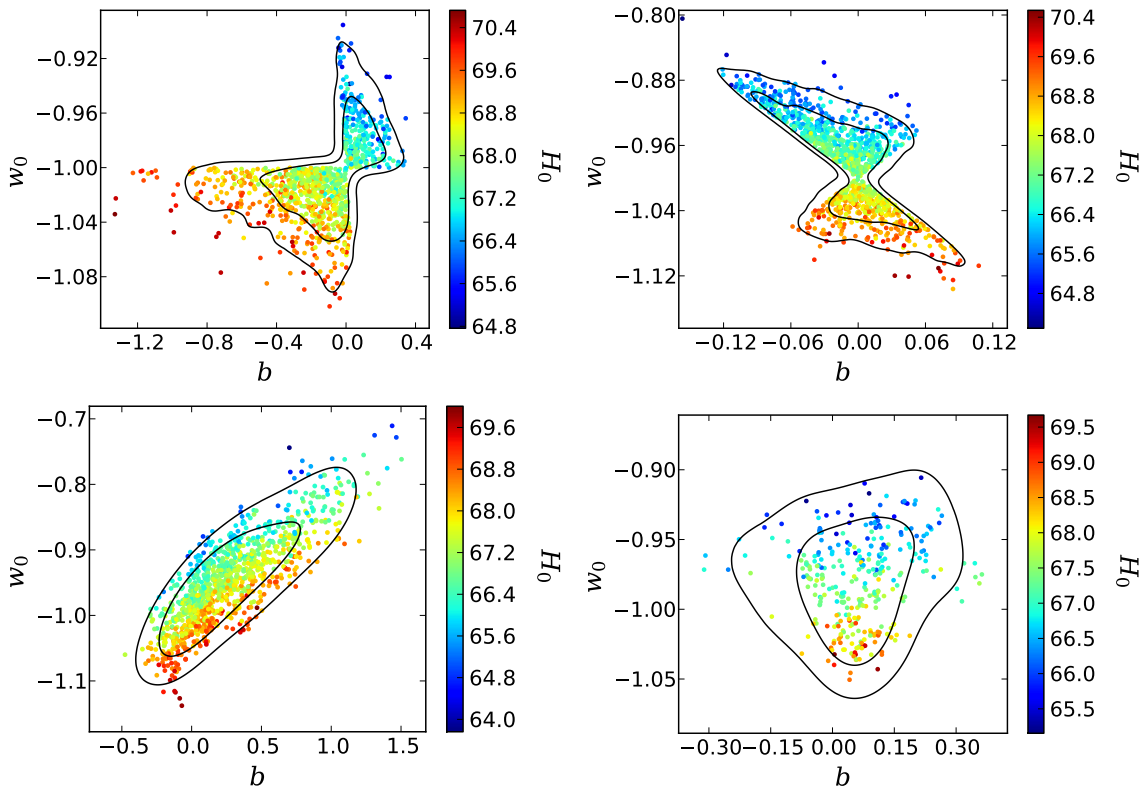


Figure 15. The trend of the key parameters (b, w_0) of the oscillating dark energy models, namely for Model I of (3.1) (upper left graph), for Model II of (3.2) (upper right graph), for Model III of (3.3) (lower left graph) and for Model IV of (3.4) (lower right graph), for different values of H_0 , from the MCMC chain of the combined analysis JLA + BAO + Planck TT, TE, EE + LowTEB + RSD + WL+ CC.

(Model I), $\ln B_{ij} = -6.2$ (Model III), $\ln B_{ij} = -8.4$ (Model IV), which implies that for all these three models we obtain a very strong preference for Λ CDM. Additionally, for Model II we acquire $\ln B_{ij} = -4.6$, which indicates the strong preference of Λ CDM over Model II. Overall, we find that Λ CDM cosmology is significantly favored compared to the examined oscillating dark energy models.

7 Conclusions

Since the nature of the dark energy sector is unknown, one can incorporate its effect in a phenomenological way, i.e. introducing various parametrizations of the dark energy equation-of-state parameter. One interesting parametrization class is the case where $w_x(z)$ exhibits oscillating behaviour [25, 29–32, 36, 37], since it may lead to interesting cosmology.

In order to thoroughly examine whether oscillating dark-energy models are in agreement with the latest observational data, we have performed a complete observational confrontation using the latest data, namely: Joint Light Curve analysis (JLA) sample from Supernovae Type Ia, Baryon Acoustic Oscillations (BAO) distance measurements, Cosmic

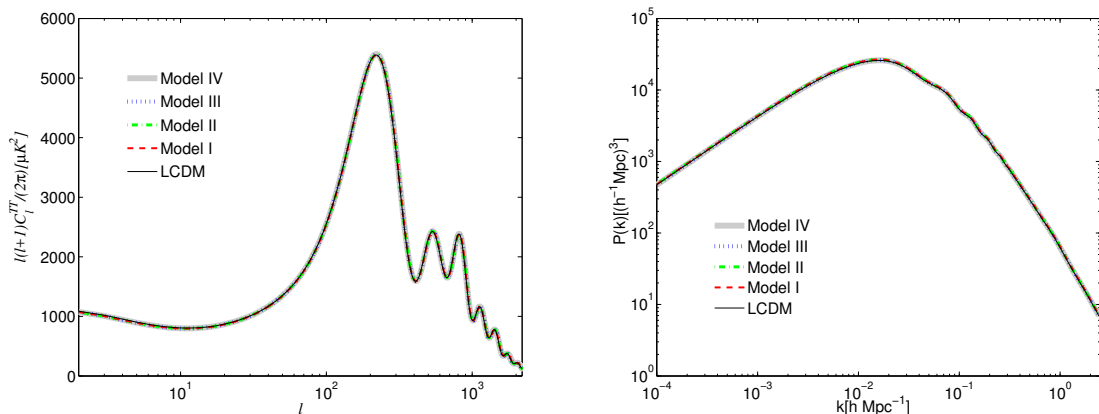


Figure 16. The temperature anisotropy in the CMB spectra (left panel) and the matter power spectra (right panel), for all Models I-IV of (3.1)-(3.4) simultaneously, for the mean values of (w_0, b) that arise from the combined analysis *JLA + BAO + Planck TT, TE, EE + LowTEB + RSD + WL+ CC*, and the corresponding curves of Λ CDM cosmology.

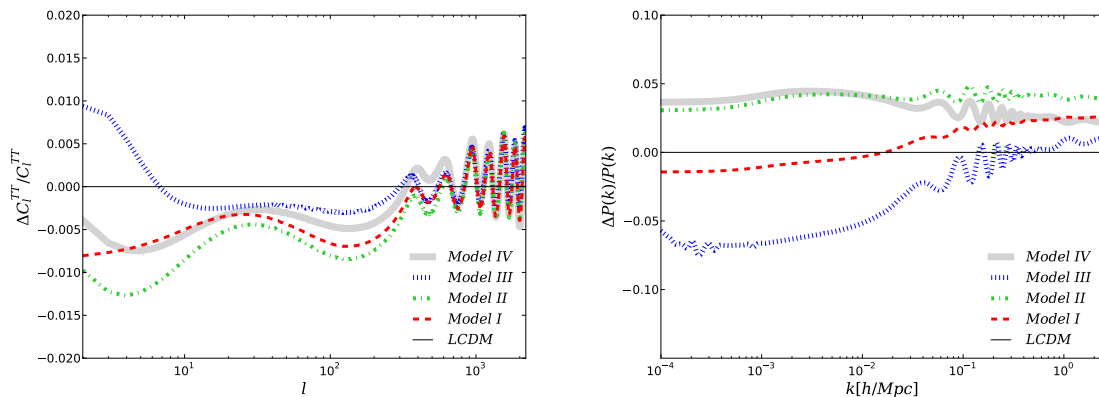


Figure 17. Relative deviation of the CMB TT spectra (left panel) and of the matter power spectra (right panel) from the Λ CDM paradigm ($b = 0$, $w_0 = -1$) for Model I of (3.1), for Model II of (3.2), for Model III of (3.3), and for Model IV of (3.4), shown for the mean values of b obtained from the combined analysis *JLA + BAO + Planck TT, TE, EE + LowTEB + RSD + WL+ CC*.

Microwave Background (CMB) observations, redshift space distortion, weak gravitational lensing, Hubble parameter measurements from cosmic chronometers, and the local Hubble constant value.

We considered four oscillating dark energy models, namely, Model I of (3.1), Model II of (3.2), Model III of (3.3) and Model IV of (3.4). Our analysis shows that for Model I, Model II and Model IV, the best fit values of the dark energy equation-of-state parameter w_0 lies in the phantom regime, nevertheless in all models the quintessential regime is also allowed within 1σ confidence-level. The models indicate deviations from Λ CDM cosmology, although such deviations are small. The fittings suggest that in all viable oscillating dark-energy models, the parameter b that quantifies the deviation from w CDM and Λ CDM

cosmology is relatively small for three models namely Model I, Model II and Model IV, while for Model III b is larger. Thus, effectively, Model III exhibits a non-zero deviation from w CDM as well as Λ CDM cosmology, however the deviation is not significant.

As a next step we analyzed the behaviour of the oscillating models at large scales, through the impact on the temperature anisotropy of the CMB spectra and on the matter power spectra. Moreover, we compared the results with the w CDM and Λ CDM scenarios, examining the corresponding deviations. As we showed, for Models II and III the deviation from w CDM and Λ CDM models is clear for large negative values of the parameter b . On the other hand, Model I exhibits a slight deviation, while for Model IV the deviation is non-significant.

Furthermore, we presented the Bayesian evidences for all oscillating dark-energy models with respect to the reference Λ CDM scenario. The results have been summarized in Table 7, from which we found that according to the present observational data Λ CDM cosmology is favored over all considered models.

We close this work with a short statistical comparison of the models, both at background and perturbative levels. In Fig. 14 we present the 1σ and 2σ confidence-level contour plots for several combinations of the free parameters and of the derived parameters, for all Models I-IV simultaneously. As we can observe, Model I is slightly different compared to the other three models, although not significantly. Moreover, we analyze the trend of the two main parameters of the oscillating models, namely b and w_0 , for different values of H_0 , using the MCMC chain of the combined analysis JLA + BAO + Planck TT, TE, EE + LowTEB + RSD + WL+ CC, and in Fig. 15 we present the results for all models. From the analysis of the MCMC chain we can clearly notice that higher values of H_0 (the red sample points in Fig. 15) favour the phantom behaviour of dark energy, while for low values of the Hubble constant H_0 (the blue sample points in Fig. 15) a quintessence-like dark energy is favored, however within 1σ , w_0 is close to -1 .

In order to examine whether these differences can be observed at large scales, in Fig. 16 we depict the temperature anisotropy in the CMB spectra (left graph) and the matter power spectra (right graph), for all models simultaneously, using for each model the corresponding mean value for the parameter b . From both graphs we deduce that we cannot distinguish the various models, and moreover all models are found to exhibit a behaviour close to that of the flat Λ CDM scenario. However, a slight difference is expected as the estimated value of b for all oscillating dark energy models is non-null. This difference can be seen in Fig. 17, in which we show the relative deviations in the CMB TT spectra (left panel) and in the matter power spectra (right panel).

In summary, the analysis of the present work reveals that the oscillating dark energy models can be in agreement with observations. However, according to the Bayesian analysis, Λ CDM cosmology is favored compared to them. One interesting extension of the above investigation would be to proceed to a more general formalism where the sound speed of the dark energy could be variable, instead of constant. This study could enlighten the intrinsic nature of the oscillating dark energy models, especially in comparison with non-oscillating models. Such an investigation is left for a future project.

Acknowledgments

We thank an anonymous referee for essential and enlightening comments that helped to improve the manuscript in a significant manner. Additionally, we are also grateful to Rafael C. Nunes and Eleonora Di Valentino for many fruitful discussions for this article. The research of SP was supported by the SERB-NPDF grant (File No. PDF/2015/000640). SP also thanks the DPS, IISER Kolkata, India, where a part of the work was finished. W. Yang's work is supported by the National Natural Science Foundation of China under Grants No. 11705079 and No. 11647153. This article is based upon work from COST Action "Cosmology and Astrophysics Network for Theoretical Advances and Training Actions", supported by COST (European Cooperation in Science and Technology).

References

- [1] E. J. Copeland, M. Sami and S. Tsujikawa, *Dynamics of dark energy*, Int. J. Mod. Phys. D **15**, 1753 (2006), [[arXiv:hep-th/0603057](#)].
- [2] Y. -F. Cai, E. N. Saridakis, M. R. Setare and J. -Q. Xia, *Quintom Cosmology: Theoretical implications and observations*, Phys. Rept. **493**, 1 (2010), [[arXiv:0909.2776](#)].
- [3] S. Nojiri and S. D. Odintsov, *Introduction to modified gravity and gravitational alternative for dark energy*, eConf C **0602061**, 06 (2006) [Int. J. Geom. Meth. Mod. Phys. **04**, 115 (2007)] [[arXiv:hep-th/0601213](#)].
- [4] S. Capozziello and M. De Laurentis, *Extended Theories of Gravity*, Phys. Rept. **509**, 167 (2011), [[arXiv:1108.6266](#)].
- [5] Y. F. Cai, S. Capozziello, M. De Laurentis and E. N. Saridakis, *$f(T)$ Teleparallel Gravity and Cosmology*, Rept. Prog. Phys. **79**, no. 10, 106901 (2016), [[arXiv:1511.07586](#)].
- [6] Y. g. Gong and Y. Z. Zhang, *Probing the curvature and dark energy*, Phys. Rev. D **72**, 043518 (2005), [[arXiv:astro-ph/0502262](#)].
- [7] M. Chevallier and D. Polarski, *Accelerating universes with scaling dark matter*, Int. J. Mod. Phys. D **10**, 213 (2001), [[arXiv:gr-qc/0009008](#)].
- [8] E. V. Linder, *Exploring the expansion history of the universe*, Phys. Rev. Lett. **90**, 091301 (2003), [[arXiv:astro-ph/0208512](#)].
- [9] A. R. Cooray and D. Huterer, *Gravitational lensing as a probe of quintessence*, Astrophys. J. **513**, L95 (1999), [[arXiv:astro-ph/9901097](#)].
- [10] P. Astier, *Can luminosity distance measurements probe the equation of state of dark energy*, Phys. Lett. B **500**, 8 (2001), [[arXiv:astro-ph/0008306](#)].
- [11] J. Weller and A. Albrecht, *Future supernovae observations as a probe of dark energy*, Phys. Rev. D **65**, 103512 (2002), [[arXiv:astro-ph/0106079](#)].
- [12] G. Efstathiou, *Constraining the equation of state of the universe from distant type Ia supernovae and cosmic microwave background anisotropies*, Mon. Not. Roy. Astron. Soc. **310**, 842 (1999), [[arXiv:astro-ph/9904356](#)].
- [13] H. K. Jassal, J. S. Bagla and T. Padmanabhan, *Observational constraints on low redshift evolution of dark energy: How consistent are different observations?*, Phys. Rev. D **72**, 103503 (2005), [[arXiv:astro-ph/0506748](#)].

- [14] E. M. Barboza, Jr. and J. S. Alcaniz, *A parametric model for dark energy*, Phys. Lett. B **666**, 415 (2008), [[arXiv:0805.1713](#)].
- [15] C. J. Feng, X. Y. Shen, P. Li and X. Z. Li, *A New Class of Parametrization for Dark Energy without Divergence*, JCAP **1209**, 023 (2012), [[arXiv:1206.0063](#)].
- [16] L. Feng and T. Lu, *A new equation of state for dark energy model*, JCAP **1111**, 034 (2011), [[arXiv:1203.1784](#)].
- [17] G. Pantazis, S. Nesseris and L. Perivolaropoulos, *Comparison of thawing and freezing dark energy parametrizations*, Phys. Rev. D **93**, no. 10, 103503 (2016), [[arXiv:1603.02164](#)].
- [18] E. Di Valentino, A. Melchiorri and J. Silk, *Reconciling Planck with the local value of H_0 in extended parameter space*, Phys. Lett. B **761**, 242 (2016), [[arXiv:1606.00634](#)].
- [19] C. Escamilla-Rivera, *Status on bidimensional dark energy parameterizations using SNe Ia JLA and BAO datasets*, Galaxies **4**, no. 3, 8 (2016), [[arXiv:1605.02702](#)].
- [20] G. B. Zhao *et al.*, “*Dynamical dark energy in light of the latest observations*”, Nat. Astron. **1**, 627 (2017), [[arXiv:1701.08165](#)].
- [21] W. Yang, R. C. Nunes, S. Pan and D. F. Mota, *Effects of neutrino mass hierarchies on dynamical dark energy models*, Phys. Rev. D **95**, 103522 (2017), [[arXiv:1703.02556](#)].
- [22] E. Di Valentino, A. Melchiorri, E. V. Linder and J. Silk, *Constraining Dark Energy Dynamics in Extended Parameter Space*, Phys. Rev. D **96**, 023523 (2017), [[arXiv:1704.00762](#)].
- [23] E. Di Valentino, *Crack in the cosmological paradigm*, Nat. Astron. **1**, 569 (2017), [[arXiv:1709.04046](#)].
- [24] W. Yang, S. Pan and A. Paliathanasis, *Latest astronomical constraints on some nonlinear parametric dark energy models*, Mon. Not. Roy. Astron. Soc. **475**, 2605 (2018), [[arXiv:1708.01717](#)].
- [25] J. Z. Ma and X. Zhang, *Probing the dynamics of dark energy with novel parametrizations*, Phys. Lett. B **699**, 233 (2011), [[arXiv:1102.2671](#)].
- [26] E. V. Linder and D. Huterer, *How many dark energy parameters?*, Phys. Rev. D **72**, 043509 (2005), [[arXiv:astro-ph/0505330](#)].
- [27] A. De Felice, S. Nesseris and S. Tsujikawa, *Observational constraints on dark energy with a fast varying equation of state*, JCAP **1205**, 029 (2012), [[arXiv:1203.6760](#)].
- [28] R. J. F. Marcondes and S. Pan, *Cosmic chronometers constraints on some fast-varying dark energy equations of state*, [[arXiv:1711.06157](#)].
- [29] V. Sahni and L. M. Wang, *A New cosmological model of quintessence and dark matter*, Phys. Rev. D **62**, 103517 (2000), [[arXiv:astro-ph/9910097](#)].
- [30] S. Dodelson, M. Kaplinghat and E. Stewart, *Solving the coincidence problem: Tracking oscillating energy*, Phys. Rev. Lett. **85**, 5276 (2000), [[arXiv:astro-ph/0002360](#)].
- [31] B. Feng, M. Li, Y. S. Piao and X. Zhang, *Oscillating quintom and the recurrent universe*, Phys. Lett. B **634**, 101 (2006), [[arXiv:astro-ph/0407432](#)].
- [32] J. Q. Xia, B. Feng and X. M. Zhang, *Constraints on oscillating quintom from supernova, microwave background and galaxy clustering*, Mod. Phys. Lett. A **20**, 2409 (2005), [[arXiv:astro-ph/0411501](#)].
- [33] J. Q. Xia, G. B. Zhao, H. Li, B. Feng and X. Zhang, *Features in Dark Energy Equation of*

- State and Modulations in the Hubble Diagram*, Phys. Rev. D **74**, 083521 (2006), [[arXiv:astro-ph/0605366](#)].
- [34] G. B. Zhao, J. Q. Xia, H. Li, C. Tao, J. M. Virey, Z. H. Zhu and X. Zhang, *Probing for dynamics of dark energy and curvature of universe with latest cosmological observations*, Phys. Lett. B **648**, 8 (2007), [[arXiv:astro-ph/0612728](#)].
- [35] S. Nojiri and S. D. Odintsov, *The Oscillating dark energy: Future singularity and coincidence problem*, Phys. Lett. B **637**, 139 (2006), [[arXiv:hep-th/0603062](#)].
- [36] D. Jain, A. Dev and J. S. Alcaniz, *Cosmological bounds on oscillating dark energy models*, Phys. Lett. B **656**, 15 (2007), [[arXiv:0709.4234](#)].
- [37] R. Lazkoz, V. Salzano and I. Sendra, *Oscillations in the dark energy EoS: new MCMC lessons*, Phys. Lett. B **694**, 198 (2010), [[arXiv:1003.6084](#)].
- [38] F. Pace, C. Fedeli, L. Moscardini and M. Bartelmann, *Structure formation in cosmologies with oscillating dark energy*, Mon. Not. Roy. Astron. Soc. **422**, 1186 (2012), [[arXiv:1111.1556](#)].
- [39] Y. Zhang, H. Zhang, D. Wang, Y. Qi, Y. Wang and G. B. Zhao, *Probing dynamics of dark energy with latest observations*, Res. Astron. Astrophys. **17**, 050 (2017), [[arXiv:1703.08293](#)].
- [40] S. Nesseris and L. Perivolaropoulos, *A Comparison of cosmological models using recent supernova data*, Phys. Rev. D **70**, 043531 (2004), [[arXiv:astro-ph/0401556](#)].
- [41] V. F. Mukhanov, H. A. Feldman and R. H. Brandenberger, *Theory of cosmological perturbations*, Phys. Rept. **215**, 203 (1992).
- [42] C. P. Ma and E. Bertschinger, *Cosmological perturbation theory in the synchronous and conformal Newtonian gauges*, Astrophys. J. **455**, 7 (1995), [[arXiv:astro-ph/9506072](#)].
- [43] K. A. Malik and D. Wands, *Cosmological perturbations*, Phys. Rept. **475**, 1 (2009), [[arXiv:0809.4944](#)].
- [44] J. K. Erickson, R. R. Caldwell, P. J. Steinhardt, C. Armendariz-Picon and V. F. Mukhanov, *Measuring the speed of sound of quintessence*, Phys. Rev. Lett. **88**, 121301 (2002), [[arXiv:astro-ph/0112438](#)].
- [45] J. Weller and A. M. Lewis, *Large scale cosmic microwave background anisotropies and dark energy*, Mon. Not. Roy. Astron. Soc. **346**, 987 (2003), [[arXiv:astro-ph/0307104](#)].
- [46] S. Hannestad, *Constraints on the sound speed of dark energy*, Phys. Rev. D **71**, 103519 (2005), [[arXiv:astro-ph/0504017](#)].
- [47] M. Betoule *et al.* [SDSS Collaboration], *Improved cosmological constraints from a joint analysis of the SDSS-II and SNLS supernova samples*, Astron. Astrophys. **568**, A22 (2014), [[arXiv:1401.4064](#)].
- [48] A. G. Riess *et al.* [Supernova Search Team], *“Observational evidence from supernovae for an accelerating universe and a cosmological constant,”* Astron. J. **116**, 1009 (1998), [[arXiv:astro-ph/9805201](#)].
- [49] D. J. Eisenstein *et al.* [SDSS Collaboration], *“Detection of the Baryon Acoustic Peak in the Large-Scale Correlation Function of SDSS Luminous Red Galaxies,”* Astrophys. J. **633**, 560 (2005), [[arXiv:astro-ph/0501171](#)].
- [50] F. Beutler *et al.*, *The 6dF Galaxy Survey: Baryon Acoustic Oscillations and the Local Hubble Constant*, Mon. Not. Roy. Astron. Soc. **416**, 3017 (2011), [[arXiv:1106.3366](#)].

- [51] A. J. Ross, L. Samushia, C. Howlett, W. J. Percival, A. Burden and M. Manera, *The clustering of the SDSS DR7 main Galaxy sample – I. A 4 per cent distance measure at $z = 0.15$* , Mon. Not. Roy. Astron. Soc. **449**, no. 1, 835 (2015), [[arXiv:1409.3242](#)].
- [52] H. Gil-Marín *et al.*, *The clustering of galaxies in the SDSS-III Baryon Oscillation Spectroscopic Survey: BAO measurement from the LOS-dependent power spectrum of DR12 BOSS galaxies*, Mon. Not. Roy. Astron. Soc. **460**, no. 4, 4210 (2016), [[arXiv:1509.06373](#)].
- [53] R. Adam *et al.* [Planck Collaboration], *Planck 2015 results. I. Overview of products and scientific results*, Astron. Astrophys. **594**, A1 (2016), [[arXiv:1502.01582](#)].
- [54] N. Aghanim *et al.* [Planck Collaboration], *Planck 2015 results. XI. CMB power spectra, likelihoods, and robustness of parameters*, Astron. Astrophys. **594**, A11 (2016), [[arXiv:1507.02704](#)].
- [55] H. Gil-Marín *et al.*, *“The clustering of galaxies in the SDSS-III Baryon Oscillation Spectroscopic Survey: RSD measurement from the power spectrum and bispectrum of the DR12 BOSS galaxies”*, Mon. Not. Roy. Astron. Soc. **465**, no.2, 1757 (2017), [[arXiv:1606.00439](#)].
- [56] C. Heymans *et al.*, *CFHTLenS tomographic weak lensing cosmological parameter constraints: Mitigating the impact of intrinsic galaxy alignments*, Mon. Not. Roy. Astron. Soc. **432**, 2433 (2013), [[arXiv:1303.1808](#)].
- [57] M. Asgari, C. Heymans, C. Blake, J. Harnois-Deraps, P. Schneider and L. Van Waerbeke, *Revisiting CFHTLenS cosmic shear: Optimal E/B mode decomposition using COSEBIs and compressed COSEBIs*, Mon. Not. Roy. Astron. Soc. **464**, 1676 (2017), [[arXiv:1601.00115](#)].
- [58] R. C. Nunes, S. Pan and E. N. Saridakis, *New constraints on interacting dark energy from cosmic chronometers*, Phys. Rev. D **94**, no. 2, 023508 (2016), [[arXiv:1605.01712](#)].
- [59] F. K. Anagnostopoulos and S. Basilakos, *“Constraining the dark energy models with $H(z)$ data: An approach independent of H_0 ,”* Phys. Rev. D **97**, no. 6, 063503 (2018), [[arXiv:1709.02356](#)].
- [60] M. Moresco *et al.*, *A 6% measurement of the Hubble parameter at $z \sim 0.45$: direct evidence of the epoch of cosmic re-acceleration*, JCAP **1605**, 014 (2016), [[arXiv:1601.01701](#)].
- [61] A. Lewis and S. Bridle, *Cosmological parameters from CMB and other data: A Monte Carlo approach*, Phys. Rev. D **66**, 103511 (2002). [[arXiv:astro-ph/0205436](#)].
- [62] R. E. Kass and A. E. Raftery, *“Bayes Factors,”* J. Am. Statist. Assoc. **90**, no.430, 773 (1995).
- [63] A. Heavens, Y. Fantaye, A. Mootoovaloo, H. Eggers, Z. Hosenie, S. Kroon and E. Sellentin, *“Marginal Likelihoods from Monte Carlo Markov Chains,”*, [[arXiv:1704.03472](#)].
- [64] A. Heavens, Y. Fantaye, E. Sellentin, H. Eggers, Z. Hosenie, S. Kroon and A. Mootoovaloo, *“No evidence for extensions to the standard cosmological model,”* Phys. Rev. Lett. **119**, no. 10, 101301 (2017), [[arXiv:1704.03467](#)].